



Self-Powered Liquid Chemical Sensors Based on Solid-Liquid Contact Electrification

Journal:	<i>Analyst</i>
Manuscript ID	AN-ART-10-2020-002126.R1
Article Type:	Paper
Date Submitted by the Author:	07-Jan-2021
Complete List of Authors:	<p>Ying, Zhihua; University of Wisconsin-Madison, Department of Materials Science and Engineering; Hangzhou Dianzi University, College of Electronics and Information</p> <p>Long, Yin; University of Wisconsin-Madison, Material Science and Engineering</p> <p>Yang, Fan; University of Wisconsin-Madison, Materials Science and Engineering</p> <p>Dong, Yutao; University of Wisconsin Madison, Material Science & Engineering</p> <p>Li, Jun; University of Wisconsin-Madison, Department of Materials Science and Engineering</p> <p>Zhang, Ziyi; University of Wisconsin Madison</p> <p>Wang, Xudong; University of Wisconsin-Madison</p>

Self-Powered Liquid Chemical Sensors Based on Solid-Liquid Contact Electrification

Zhihua Ying^{1,2*}, Yin Long¹, Fan Yang¹, Yutao Dong¹, Jun li¹, Ziyi Zhang¹, Xudong Wang^{1*}

¹ Department of Materials Science and Engineering, University of Wisconsin-Madison,
Madison, WI 53706, United States

² College of Electronics and Information, Hangzhou Dianzi University, Hangzhou, 310018,
People's Republic of China

Email: X.W.: xudong.wang@wisc.edu; Z.Y.:yingzh@hdu.edu.cn

Keywords: Tribo-electrification; liquid-solid interface; amino acids; liquid sensing; self-power.

Abstract

Triboelectric nanogenerators (TENG) have attracted many research endeavors as self-powered sensors for force, velocity, and gas detections based on solid-solid or solid/air interactions. Recently, triboelectrification at liquid-solid interfaces also showed intriguing capability in converting the physical contacts into electricity. Here, we report a self-powered triboelectric sensor for liquid chemical sensing based on liquid-solid electrification. As a liquid droplet passed across the tribo-negative sensor surface, the induced surface charge balanced with the electrical double layer charge in the liquid droplet. The competing between the double layer charge and surface charge generated characteristic positive and negative voltage spikes, which may serve as a “binary feature” to identify the chemical compound. The sensor showed distinct features to three amino acids including glycine, lysine and phenylalanine as a function of their concentration. The versatile sensing ability was further demonstrated on several other inorganic and organic chemical

1
2
3 compounds dissolved in DI water. This work demonstrated a promising sensing application based
4
5 on the triboelectrification principle for biofluid sensor development.
6
7
8
9

10 **Introduction**

11
12 Liquid sensing is broadly utilized in many areas including chemical industry [1-3], medical
13 diagnosis [4-6], food manufacturing [7-9], and environmental protection [10-13]. Currently, the most
14 commonly used methods for detecting biochemical concentrations in liquids are based on
15 electrochemical sensors [14-17], fluorescent probes [18-20] and optical fiber sensors [21,22]. These
16 devices are typically bulky, complex, run on an external power source, and require relatively long
17 time to obtain required information. It is generally desired for a liquid sensor to provide a rapid,
18 continuous and reliable detection. Recently, contact electrification between liquid and solid films
19 has been demonstrated as a promising methodology for inducing electric charges on solid surfaces
20 [23-25]. This phenomenon quickly becomes an intriguing design principle of triboelectric
21 nanogenerator (TENG) for direct electricity generation from liquid movements, such as rain drops
22 and water waves [26-28]. Same as other TENG devices, a self-powered liquid chemical sensor can
23 generate electrical signals through the triboelectric effect without any extra energy supply. This
24 signal information could be directly sent to other electronics in real applications[29-31]. Thus, this
25 immediate electricity-generation capability from liquid motion allows implementation of this
26 principle as a power-free sensor device that would be simple, portable or wearable, and cost
27 effective [32-34].
28
29
30
31
32
33
34
35
36
37
38
39
40
41
42
43
44
45
46
47
48

49 A two-step formation process of the electric double layer (EDL) at the liquid-solid interface
50 has proposed by Wang^[35, 36], and electron transfer dominates on some materials. Based on the
51 electrification principle, the amount of electricity generated is dependent on the dielectric property
52
53
54
55
56
57
58
59
60

1
2
3 and the electronegativity of both the liquid and contacting material as well as the area of contacting
4 surface and the moving speed. Thus far, studies were primarily focused on how to optimize the
5 solid materials in order to improve the electricity generation from water droplets [23,37-41]. However,
6 with given physical conditions of a liquid-solid interactive TENG, it is reasonable to envision that
7 the change of liquid composition would also induce electric output variations^[42,43]. This type of
8 change, if quantified, can provide an ideal sensing capability for liquid samples, which may offer
9 profound application potentials in liquid chemical sensing, biofluid sensing, and environmental
10 sensing. In this article, we report a simple self-powered liquid sensor for chemical sensing based
11 on the principle of liquid-solid contact electrification. The triboelectrification (TE)-based sensor
12 device showed a fast sensitivity to various biochemicals including glycine, lysine, phenylalanine,
13 and interference chemicals dissolved in water. This study successfully validated the hypothesis
14 that the liquid contact electrification may bring a new liquid sensing strategy for portable, wearable
15 and self-powered biofluid sensor development.

35 **Results and discussion**

36
37 The working principle of the self-powered biofluid sensor is based on the contact
38 electrification principle between the testing liquid droplets and the PTFE surface. As illustrated in
39 Fig. 1A, the sensor surface was a PTFE thin film for liquid reception. Two copper electrodes on
40 the back side were set for outputting the triboelectric voltage signal. Electrode at the lower position
41 was the sensing electrode to collect electrification-induced charges; while the top electrode was
42 used as the reference electrode. Water charge is always positive but its magnitude is related to the
43 material position in most triboelectric series, where PTFE is a highly negative material^[44, 45], when
44 a liquid droplet contacts the PTFE surface, negative charges are induced at the PTFE surface and
45
46
47
48
49
50
51
52
53
54
55
56
57
58
59
60

1
2
3 the droplet becomes positively charged. Opposite charges could also form in the vicinity of the
4 charged liquid surface as an electrochemical double layer. During the initial movement of liquid
5 droplet, local charges will establish an equilibrium distribution, where the positive liquid surface
6 charge is balanced by PTFE surface charge (σ_s) and liquid internal charge (σ_l) (Fig. 1A-I). As the
7 droplet moves over the electrode covered area, the negative charges on PTFE surface induces
8 positive charge on sensing electrode, generating a positive voltage peak over a load connected
9 between the sensing and reference electrodes (Fig. 1A-II). Once the droplet passes the sensing
10 electrode region, the induced charges become unbalanced, and thus a negative potential difference
11 builds up to drive electrons back to the sensing electrode. This local electronic fluctuation may
12 also disturb the electrochemical double layer distribution, and thus release more positive charges
13 to be balanced by the sensing electrode (Fig. 1A-III). Therefore, larger amount of charges (or high
14 local potential) could be induced in this stage compared to stage II. The electric equilibrium will
15 eventually be re-established after the droplet moves away from the sensing area (Fig. 1A-IV).
16 Corresponding voltage output profile of one cycle is shown in Fig. 1B, illustrating a biphasic
17 waveform with a significantly higher negative voltage peak value compared to the positive peak.
18 Integrating the peak area representing the amount of charge following through the load, which also
19 revealed the charge flow in stage III was about twice as much as those in stage II. Besides, the
20 time (Δt) from 0 V to the maximal value only took 0.02s, demonstrating a fast sensing response.
21
22
23
24
25
26
27
28
29
30
31
32
33
34
35
36
37
38
39
40
41
42
43
44

45 Based on the mechanism, the voltage peak intensity would be related to the time that the
46 liquid droplet passed the electrode area, *or* how fast the charges may be balanced. To reveal this
47 relationship, the moving speed was controlled by tilting the sensor plate at different angle. First, it
48 was found that the both positive and negative voltage peaks were rather stable as the tilting angle
49 was fixed. At a tilting angle of 30°, the average negative voltage peaks were -0.020 ± 0.001 V. The
50
51
52
53
54
55
56
57
58
59
60

1
2
3 small voltage amplitude was likely due to the slow motion of the droplet, which induced a slow
4 charge accumulation. As the tilting angle increased to 45° , the average negative voltage peaked at
5
6 -0.116 ± 0.008 V, which was only slightly decreased to -0.096 ± 0.010 V as the tilting angle
7
8 increased to 60° and then rapidly dropped to -0.014 ± 0.002 V at the tilting angle of 75° . However,
9
10 the positive voltage peaks remained at a fairly stable value of ~ 0.02 V from all these tilting angles
11
12 (Fig. 2A). The nearly constant positive peaks evidenced the reach of equilibrium state before the
13
14 droplet arriving at the sensing electrode, and thus nearly the small amount of charge would be
15
16 induced in stage II. The significantly enhanced negative peak intensity at 45° suggested that
17
18 appropriate time of interaction between the droplet and sensing electrode was needed to maximize
19
20 the charge to be released from the double layer trapping. The rapid drop of the negative voltage at
21
22 higher tilting angle could be attributed to the insufficient interaction for releasing the trapped
23
24 charge. This result proved that droplet travel speed was an important factor that controlled the
25
26 voltage output. Therefore, in order to obtain the maximum output signal of sensing response, all
27
28 the sensing experiments were conducted at 45° tilting angle (the velocity was quantified by an
29
30 alternative design, Supporting information S2), and 1.25 ± 0.23 nA tribo-current was obtained as
31
32 shown in Fig.S3. By applying droplets repeatedly from the same position, consistent voltage
33
34 outputs of -0.1 ± 0.01 V were obtained. This process was repeated over five different times, and
35
36 the voltage output exhibited a nearly constant value from each group of measurements with a
37
38 variation within 3% of the signal value (Fig. 2B), confirming the good repeatability of the sensing
39
40 responses. It should be noted that although the contact area of a droplet and PTFE may be also
41
42 affected by the tiling angle^[46], it had negligible impact to moving speed quantification. This is
43
44 because the speed was only determined by the time difference between the two voltage peaks when
45
46
47
48
49
50
51
52
53
54
55
56
57
58
59
60

1
2
3 the liquid droplet passed the two electrodes, and the distance between the two electrodes, which
4 were not affected by the contact area.
5
6

7
8 The voltage generation mechanism suggests that the amount of induced charge was also
9 related to the relevant electronegativity of the liquid droplet compared to PTFE. Many other
10 physical conditions, such as the tilting angle, flowing distance, and droplet volume would change
11 the voltage amplitude. When all these conditions were fixed, the results would be able to reflect
12 the (di)electric property of the droplet, and thereby providing a selective sensing capability. Here,
13 we select amino acids, a group of very important biological substance,^[47-49] as an example to show
14 the self-powered selective sensing capability of the TE-based liquid sensors. Three essential amino
15 acids (Table S2) were selected for two reasons: structure and biomedical applications, and
16 significance of disease diagnosis. Glycine, the one with the simplest chemical structure in amino
17 acids, has anti-inflammatory and immunomodulatory function, and is also an insulin
18 secretagogue.^[50] Lysine, the one with aliphatic side chain, is considered as a potential biomarker
19 for renal cell carcinoma, and plays a key role in the neurotoxicity of amyloid b-protein in
20 Alzheimer's disease (AD).^[51] Phenylalanine, the one with aromatic side chain, is related to immune
21 activation in the pathogenesis of AD.^[52,53] Therefore, these three types of amino acids are
22 representative and adequate to support the hypothesized sensing capability.
23
24
25
26
27
28
29
30
31
32
33
34
35
36
37
38
39
40
41

42 In order to quantitatively evaluate the performance of TE-based sensor for the selected amino
43 acids, the voltage outputs were recorded from amino acids droplets with different concentrations.
44 The highest concentration was chosen according to the solubility of the specific amino acids. Each
45 measurement on each concentration value was conducted for at least 15 seconds (i.e.20 droplets).
46 For comparison, DI water droplets were also tested with each group of amino acid samples. As
47 shown in Figure 3, the DI water droplets yielded the highest negative voltage peak at ~ -0.1 V
48
49
50
51
52
53
54
55
56
57
58
59
60

1
2
3 compared to all three amino acid samples. Significant changes in the negative voltage peaks were
4
5 observed as the concentration changes; while the positive peaks remained a fairly small range of
6
7 variation. In general, both positive and negative voltage peaks decreased as the concentration
8
9 increased for all amino acids (Figure 3A-C). The negative voltage peaks exhibited a significantly
10
11 larger change compared to the positive voltage peaks. As shown in Figure 3D-F, the average
12
13 negative voltage peak values at each concentration point were plotted for each amino acid and well
14
15 fitted to a logarithm curve (Table S3). As the positive peak intensity was directly related to σ_s ,
16
17 increase the amino acid concentration had little impact to the balanced σ_l and σ_s values. Therefore,
18
19 the positive peak intensity showed very small variation (decreasing) as the amino acid
20
21 concentration increased across the entire testing range. The large decrease of negative voltage peak
22
23 intensity could be attributed to the stabilization of the electrochemical double layer in the liquid
24
25 droplet when additional amount of amino acid was added. The ratio of the positive to negative
26
27 peak intensity were all eventually reaching a unit, suggesting an equal amount of charge flow was
28
29 established at high concentrations. This phenomenon revealed that as the double layer was
30
31 eventually stabilized, both back and forth charge flows were only contributed to σ_s .
32
33
34
35
36
37

38 One should notice that although the general principle was the same and so as similar trends
39
40 were obtained, the three amino acids demonstrated distinguishing voltage change patterns. The
41
42 changing rate as well as the ratio between positive and negative peak value, would reflect the
43
44 molecules chemical and dielectric natural. Therefore, these two patterns together may be
45
46 considered as a “binary feature” to identify the molecules. Compared to lysine and phenylalanine,
47
48 glycine has a relative simple chemical structure and does not have any large side chains (Table
49
50 S2). Since the $-\text{NH}_2$ group is always positively charged in a solution, more $-\text{NH}_2$ groups in the
51
52 molecule would yield more or stronger electric dipoles in the solution when triboelectric charges
53
54
55
56
57
58
59
60

1
2
3 were induced. Therefore, as the droplet moved away from the sensing electrode, more/stronger in-
4 solution dipoles would bring a stronger interaction at the droplet surface and stabilized the induced
5 surface charge (σ_1), thus the obtained highest sensitivity also could be found in Fig. S5. As less σ_1
6 being released, the negative peak would be more relative to σ_s and thus closer to the value of
7 positive peak, moving their ratio closer to unit. The presence of nonpolar and large aromatic side
8 chain in phenylalanine could be the reason for the most significant decrease of the positive peak
9 as its concentration increase.

19 The results above revealed that increase in ion concentration leads to the suppression of the
20 transferred charge amount. To further demonstrate the strong and versatile sensing ability of our
21 TE-based liquid sensor, we tested the voltage responses from a broader range of chemicals,
22 including Ethanol, NaCl, Acetic acid, PBS and Na₂CO₃. Urea, a breakdown product of amino acids,
23 was not selected because it is neither acidic nor alkaline when dissolves in water. All of these
24 solutions were prepared with a concentration of 0.1 mol/L in DI water. DI water and tap water
25 (which contains several types of ions) were also detected for comparison. The corresponding
26 voltage output profiles are shown in Fig. 4A. It could be seen that DI water still had the maximum
27 voltage output due to the minimal free ions in the solution, as expected. Similar voltage profile
28 (with a slight decrease in negative voltage peak) was obtained from ethanol solution, possibly due
29 to their similar protic behavior. Tap water, as it contained a lot more free ions, generated a much
30 lower negative voltage peak compared to those from DI water droplets. The three ionic solutions,
31 NaCl, Acetic acid and Na₂CO₃, exhibited the lowest voltage peaks, both negative and positive, and
32 their ratios were nearly unit as shown in Fig.4B. This phenomenon is consistent with our proposed
33 mechanism that free ions stabilized the double layer in liquid droplet (*i.e.* σ_1), and the negative
34 voltage was largely determined by σ_s alone.

Conclusions

In summary, we developed a self-powered triboelectric sensor based on liquid-solid electrification for liquid chemical sensing. The sensor was built on a triboelectric negative surface with two back Cu electrodes for charge induction. As the liquid droplet passed over the sensor surface, positive charges were induced at the liquid surface, which were balanced by the electrical double layer charge in the liquid and the surface charge from the sensor. As the liquid droplet passing through the sensing electrode, the competing releasing of the double layer charge and surface charge generated characteristic positive and negative voltage spikes, which signaled the liquid chemistry. We tested the sensing responses to three different types of amino acids, including glycine, lysine and phenylalanine. The negative voltage peaks demonstrated a strong concentration relationship, which decreased logarithmically as the concentration increase. We further showed the sensor behavior to several organic and inorganic chemicals. The characteristic negative and positive voltage peaks and their amplitude ratio also confirmed the strong correlation to free ion concentrations. Therefore, we believe that in our triboelectric liquid sensor, the multiple sources of surface charge generation and balancing could provide distinct positive and negative voltage output directly correlating to the liquid chemistry. This phenomenon may potentially serve as a “binary feature” for chemistry identification in liquid solution with more comprehensive quantification. This liquid sensor design, together with its surface-charge-determined sensing principle, offers a great promise for the development of effective and low-cost sensor technology for liquid systems.

Experimental section

1
2
3 **Materials.** Glycine (98.5+%), L-lysine ($\geq 98\%$), L-Phenylalanine ($\geq 98\%$), Acetic acid
4 ($\geq 98\%$) and Sodium Carbonate (Na_2CO_3 , $\geq 99.5\%$) were purchased from Millipore Sigma Co..
5
6 Sodium Chloride (NaCl , $\geq 99.0\%$) was obtained from Alfa Aesar Co.. Ethyl alcohol 200 Proof was
7
8 purchased from Pharmco by Greenfield Global Inc.. Phosphate buffered saline (PBS, Tissue
9
10 Culture Grade) was purchased from Crystalgen Inc.. Polytetrafluoroethylene (PTFE) film was
11
12 obtained from CS Hyde Co..
13
14
15

16
17 **Fabrication of the self-powered liquid sensor.** The method used to fabricate the TENG-
18
19 based sensor is depicted in Fig. S1. A rectangular PTFE film (90 μm in thickness, 1 cm wide and
20
21 7 cm long) was washed in acetone, ethanol and DI water for 15 min each. Two Cu electrodes 22 μm
22
23 in thickness were deposited by E-beam Evaporation (CHA-600) on the backside of the PTFE film.
24
25 The top Cu electrode had a size of 0.2 cm \times 0.5 cm and the lower Cu electrode was 1 cm \times 0.5 cm
26
27 in size. The two Cu electrodes were spaced by 5 cm. The top electrode was positioned in the middle
28
29 of the PTEF film to avoid direct liquid droplets contact.
30
31
32

33 **Sensor characterization.** As shown in Fig. S3, a separating funnel (125 mL in volume)
34
35 was used to contain the liquid sample and provide continuous liquid droplets toward the PTFE
36
37 film with a stable dropping frequency. The funnel outlet was positioned 0.5 cm above the PTFE
38
39 film, and 0.5 cm ahead of the first Cu electrode. The droplets came out of the funnel outlet all had
40
41 a consistent volume of 0.05 ml. The voltage outputs of the TE-based sensor between the two Cu
42
43 electrodes were measured by a low-noise amplifier (Stanford research systems, Model SR560).
44
45 Contact angles were tested using a Dataphysics OCA 15 Optical Contact Angle Measuring System.
46
47 A Zeiss LEO 1530 Schottky-type field-emission scanning electron microscope was used to image
48
49 the morphologies of the samples.
50
51
52
53
54
55
56
57
58
59
60

Author contributions

Zhihua Ying: Conceptualization, Methodology, Visualization, Data curation, Writing - original draft. Yin Long: Conceptualization, Methodology, Writing - original draft. Fan Yang: Validation, Software. Yutao Dong: Conceptualization. Jun li: Methodology. Ziyi Zhang: Investigation. Xudong Wang: Conceptualization, Methodology, Supervision, Writing - review & editing.

Conflicts of interest

There are no conflicts to declare.

Acknowledgements

This work was primarily supported by the National Science Foundation DMR-1709025. Z. Y. is grateful for the financial support from China Scholarship Council.

References

1. C. Bai, J. Zhang, R. Quo, Q. Zhang, M. Mei, M. Chen, B. Wei, C. Wang and C. Qu, *Ind. Eng. Chem. Res.* 2020, **59**, 8125-8135
2. R. Boroujerdi, A. Abdelkader and R. Paul, *Nano-Micro Lett.*, 2020, **12**, 33
3. B. Huy, H. P. Van, D. V. Pham, T. H. C. Hoang, T. B. Pham, T. C. Do, Q. M. Ngo and T. V. Nguyen *Environ. Technol. Lett.*, 2019, **40**, 3403-3411
4. S. Rassel, C. Xu, S. Zhang and D. Y. Ban, *Anal.*, 2020, **145**, 2441-2456
5. Q. Fan, L. Wang, D. Xu, Y. Duo, J. Gao, L. Zhang, X. Wang, X. Chen, J. Li and H. Zhang, *Nanoscale*, 2020, **12**, 11364-11394
6. Y. M. Park, Y. S. Choi, H. R. Lee, Y. S. Heo, N. H. Bae, T. J. Lee and S. J. Lee, *Biosens. Bioelectron.*, 2020, **161**, 112252
7. F. Laghrib, M. Bakasse, S. Lahrich and M. A. El Mhammedi, *Mater. Sci. Eng. C*, 2020, **107**, 110349

- 1
- 2
- 3 8. O. Cakir, M. Bakhshpour, F. Yilmaz and Z. Baysal, *Mater. Sci. Eng. C*, 2019, **102**, 483-491
- 4
- 5 9. H. Mahmoudi-Moghaddam, S. Tajik, and H. Beitollahi, *Food. Chem.*, 2019, **286**, 191-196
- 6
- 7 10. L. Yang, Y. L. Liu, C. G. Liu, F. Ye and Y. Fu, *J. Hazard. Mater.*, 2020, **381**, 120966
- 8
- 9 11. E. Shojaei, M. Masrournia, A. Beyramabadi and H. Behmadi, *Int. J. Environ. Anal. Chem.* 2020, **3**, 1-
- 10 16
- 11
- 12 12. X. Fang, B. Zong, and S. Mao, *Nano-Micro Lett.* 2018, **10**, 64
- 13
- 14 13. G. Chakraborty, P. Das, and S. K. Mandal, *ACS Appl. Mater. Interfaces* 2018, **10**, 49, 42406–42416
- 15
- 16 14. Y. Yao, X. X. Liu, Y. Z. Shao, Y. B. Ying and J. F. Ping, *Biosens. Bioelectron.*, 2020, **66**, 112463
- 17
- 18 15. P. Singh, S. K. Pandey, J. Singh, S. Srivastava, S. Sachan and S. K. Singh, *Nano-Micro Lett.*,
- 19 2016, **8**, 193–203
- 20
- 21
- 22 16. F. Li, Z. Yu, X. Han and R. Lai, *Anal. Chim. Acta*, 2019, **1051**, 1-23
- 23
- 24 17. Y. Zhang and X. Chen, *Nanoscale*, 2019, **11**, 19105-19118
- 25
- 26 18. H. Qi, M. Teng, M. Liu, S. Liu, J. Li, H. Yu, C. Teng, Z. Huang, H. Liu, Q. Shao, A. Umar, T. Ding,
- 27 Q. Gao and Z. Guo, *J. Colloid Interface Sci.*, 2019, **539**, 332-341
- 28
- 29 19. Y. Wang, S. Lao, W. Ding, Z. Zhang and S. Liu, *Sens. Actuat. B-Chem.*, 2019, **284**, 186-192
- 30
- 31 20. X. Wu, H. Wang, S. Yang, H. Tian, Y. Liu and B. Sun, *Food Chem.*, 2019, **284**, 23-27
- 32
- 33 21. Y. Zhang, Y. Sun, L. Cai, Y. Gao and Y. Cai, *Meas.* 2020, **158**, 107742
- 34
- 35 22. Y. Zhang, T. Zhou, B. Han, A. Zhang and Y. Zhao, *Nanoscale*, 2018, **10**, 13832-13856
- 36
- 37 23. D. Choi, D. W. Kim, D. Yoo, K. J. Cha, M. La and D. S. Kim, *Nano Energy*, 2017, **36**, 250–259
- 38
- 39 24. W. Tang, B. D. Chen and Z. L. Wang, *Adv. Funct. Mater.*, 2019, 1901069
- 40
- 41 25. S. Chatterjee, S. R. Burman, I. Khan, S. Saha, D. Choi, S. Lee and Z.-H. Lin, *Nanoscale*, 2020, **12**,
- 42 17663-17697
- 43
- 44 26. W. Xu, H. Zheng, Y. Liu, X. Zhou, C. Zhang, Y. Song, X. Deng, M. Leung, Z. Yang, R. X. Xu, Z. L.
- 45 Wang, X. C. Zeng and Z. Wang, *Nature*, 2020, **578**, 392–396
- 46
- 47 27. Y. Long, Y. Yu, X. Yin, J. Li, C. Carlos, X. Du, Y. Jiang and X. Wang, *Nano Energy*, 2019, **57**, 558-
- 48 565
- 49
- 50
- 51
- 52
- 53
- 54
- 55
- 56
- 57
- 58
- 59
- 60

- 1
2
3 28. G. Zhu, Y. Su, P. Bai, J. Chen, Q. Jing, W. Yang and Z. L. Wang, *ACS Nano*, 2014, **8**, 6, 6031–6037
4
5 29. X. Li, M. H. Yeh, Z.H. Lin, H. Guo, P. K. Yang, J. Wang, S. Wang, R. Yu, T. Zhang and Z. L. Wang,
6
7 *ACS Nano*, 2015, **9**, 11, 11056–11063
8
9 30. L. Zheng, Y. Wu, X. Chen, A. Yu, L. Xu, Y. Liu, H. Li and Z. L. Wang, *Adv. Funct. Mater.* 2017, **27**,
10
11 1606408
12
13 31. H. Wang, Z. Xiang, P. Giorgia, X. Mu, Y. Yang, Z. L. Wang and C. Lee, *Nano Energy*, 2016, **23**, 80–
14
15 88
16
17 32. S. Jang, M. La, S. Cho, Y. Yun, J. H. Choi, Y. Ra, S. J. Park and D. Choi, *Nano Energy*, 2020, 70,
18
19 104541
20
21 33. Z. Yuan, X. Du, H. Niu, N. Li, G. Shen, C. Li and Z. L. Wang, *Nanoscale*, 2019, **11**, 495–503 2019
22
23 34. W. Tang, T. Jiang, F. Fan, A. Yu, C. Zhang, X. Cao and Z. L. Wang, *Adv. Funct. Mater.*, 2015, **25**,
24
25 3718-3725
26
27 35. Z. L. Wang and A. C. Wang. *Mater. Today*, 2019, **30**, 34-51
28
29 36. S. Lin, X. Chen and Z. L. Wang, *Nano Energy*, 2020, **76**, 105070
30
31 37. Y. Wang and Y. Yang, *Nano Energy*, 2019, **56**, 547-554
32
33 38. X. Chen, Q. Xu, S. Bai and Y. Qin, *Nano Energy*, 2017, **33**, 288-292
34
35 39. L. Zhang, N. Zhang, Y. Yang, S. Xiang, C. Tao, S. Yang and X. Fan, *ACS Appl. Mater. Interfaces*,
36
37 2018, **10**, 36, 30819–30826
38
39 40. X. Cui, H. Zhang, S. Cao, Z. Yuan, J. Ding and S. Sang, *Nano Energy*, 2018, **52**, 71–77
40
41 41. Z. H. Lin, G. Cheng, S. Lee, K. C. Pradel and Z. L. Wang, *Adv. Mater.*, 2014, **26**, 4690–4696
42
43 42. S. Lin, L. Xu, A. C. Wang and Z. L. Wang. *Nat. Commun.*, 2020, 11, 399
44
45 43. J. Nie, Z. Ren, L. Xu, S. Lin, F. Zhan, X. Chen and Z. L. Wang. *Adv. Mater.*, 2019, 1905696
46
47 44. T. A. L. Burgo, F. Galembeck and G. H. Pollack, *J. Electrostat.* 2016, 80, 30-33
48
49 45. P. Jiang, L. Zhang, H. Guo, C. Chen, C. Wu, S. Zhang and Z. L. Wang, *Adv. Mater.*, 2019, 1902793
50
51 46. I. Ríos-López, S. Evgenidis, M. Kostoglou, X. Zabulis and T. D. Karapantsios, *Colloid Surface A*,
52
53 2018, **549**, 164–173
54
55
56
57
58
59
60

- 1
2
3 47. F.S. Mjalli, *J. Taiwan Inst. Chem. Eng.*, 2016, **61**, 64-74
4
5 48. H. Uneyama, H. Kobayashi and N. Tonouchi, *Biochem. Eng. Biotechnol.*, 2017, **159**, 273-287
6
7 49. S. Dato, E. Hoxha, P. Crocco, F. Iannone, G. Passarino and G. Rose, *Biogerontol.*, 2019, **20**, 17-31
8
9 50. M. Zenil-Vega, E. Ceron, G. Lopez-Bello, J. Moreno, E. Juarez-Cruz, M. Castillejos-Lopez, D. Bernal-
10 Alcantara, B. Sommer, and N. Alvarado-Vasquez, *Clin. Nutr.*, 2020, **39**, **10**, 3019-3023.
11
12 51. A. Arendowski and T. Ruman, *Anal. Methods*, 2018, **10**, 5398-5405
13
14 52. P. Wissmann, S. Geisler, F. Leblhuber and D. Fuchs, *J. Neurol. Sci.*, 2013, **329**, 29-33
15
16 53. N. Ermiş, L. Uzun and A. Denizli, *J. Electroanal. Chem.*, 2017, **807**, 244–252
17
18
19
20
21
22
23
24
25
26
27
28
29
30
31
32
33
34
35
36
37
38
39
40
41
42
43
44
45
46
47
48
49
50
51
52
53
54
55
56
57
58
59
60

Figures and Captions

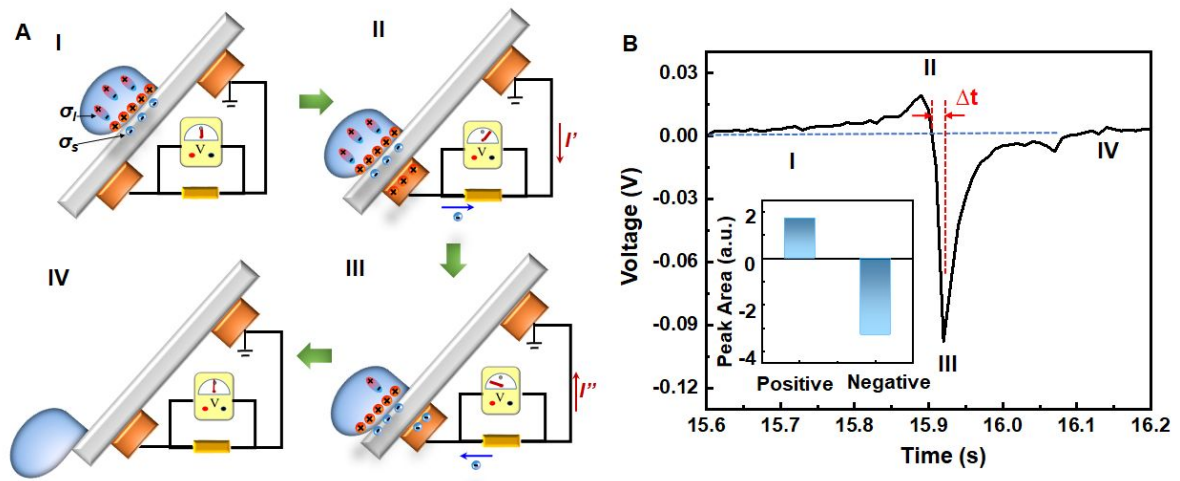


Figure 1. Mechanism of TE-based liquid sensor. **A.** Schematic illustration of the working principle of the TE-based sensor as a liquid droplet flowing by the sensor surface. **B.** A typical voltage output profile of the TE-based sensor under the flow of one single water droplet. Inset is integrated peak area under positive and negative voltage peaks.

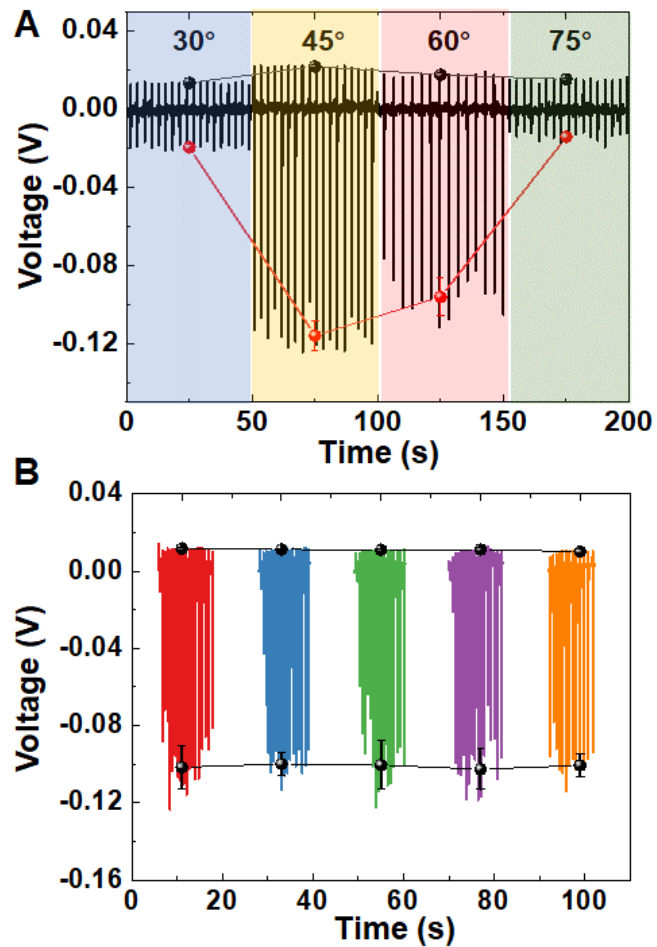


Figure 2. Voltage signal of the TE-based liquid sensor. A. Voltage signals of a TE-based liquid sensor at different tilting angles. **B.** Repeated voltage output signal recorded from the TE-based sensor at 45 ° tilting angle for five different times.

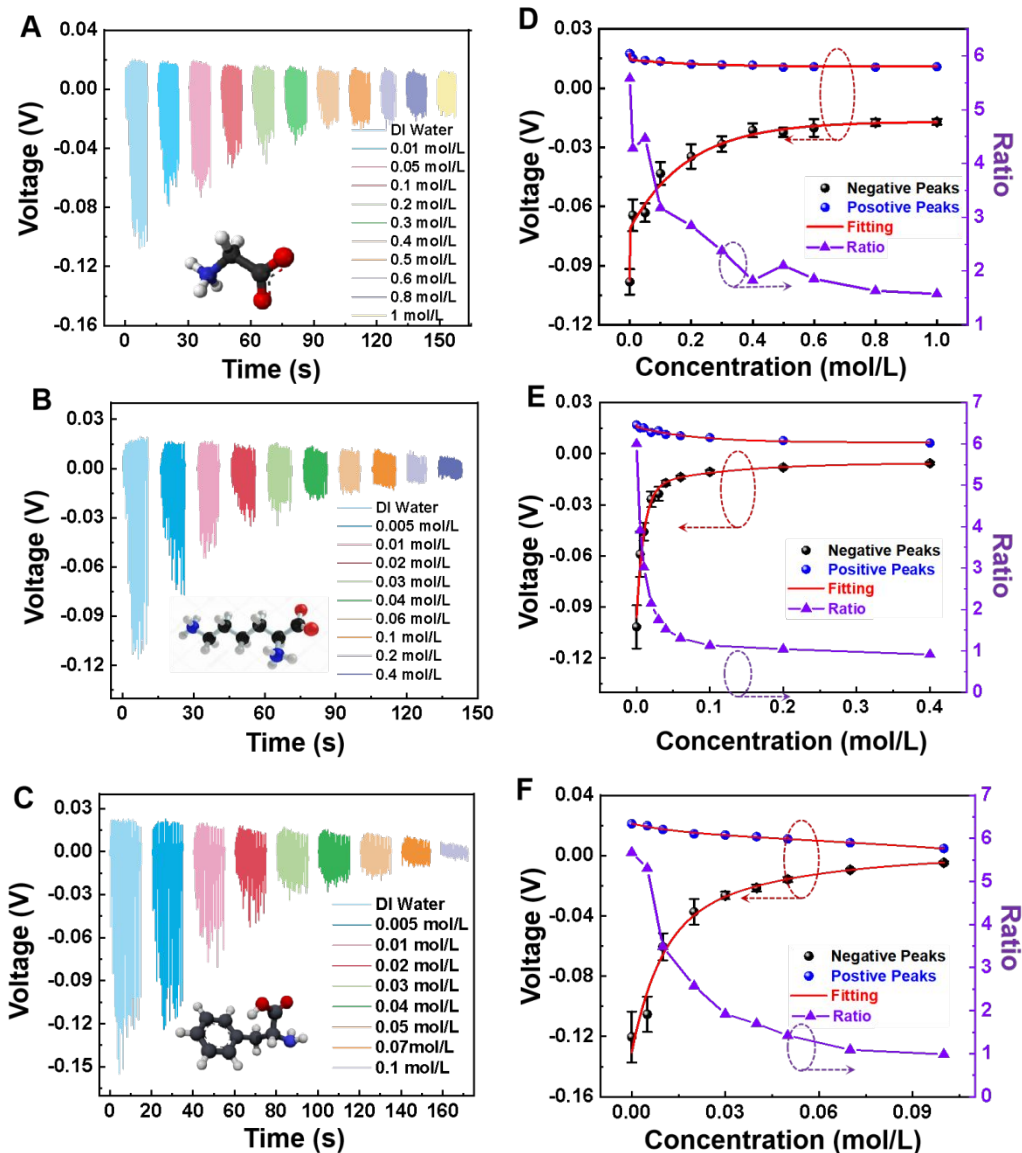


Figure 3. Voltage responses of the TE-based liquid sensor to three amino acids. The voltage output signals of the TE-based sensor to glycine (A), lysine (B) and phenylalanine (C) aqueous solutions measured at a series of concentrations, respectively. (D-F) Corresponding plot of the voltage peak values as a function of concentration for glycine, lysine, and phenylalanine, respectively.

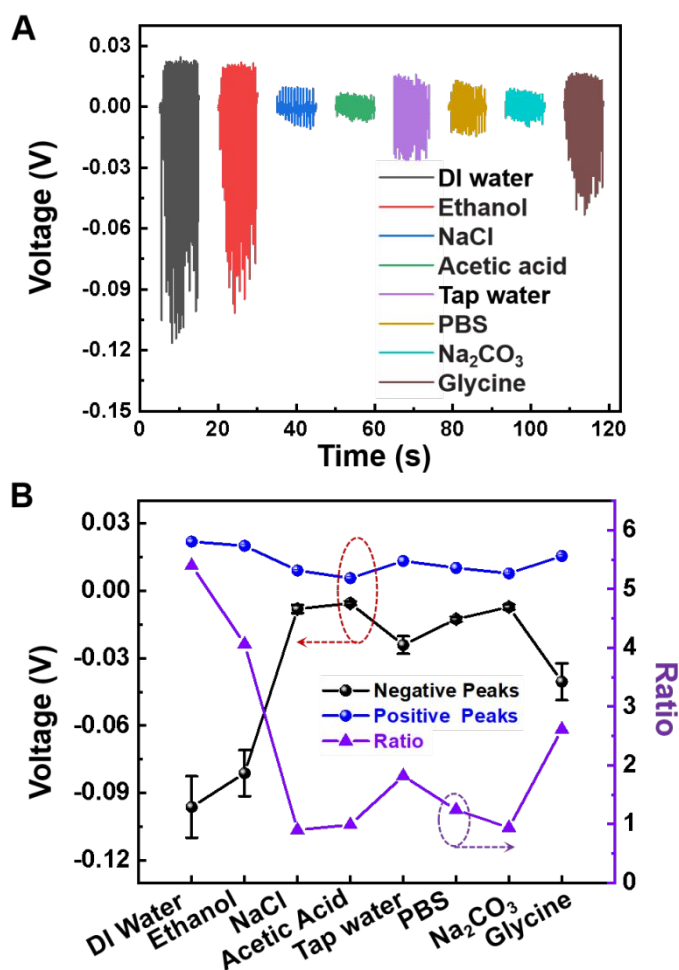


Figure 4. Sensing capability of a TE-based liquid sensor to different analytes. A. Voltage response of the TE-based liquid sensor when droplets of DI water, Ethanol, NaCl, Acetic acid, Tap water, PBS, Na₂CO₃ and Glycine were added to the sensor surface. Except water, other analytes were prepared with a concentration of 0.1 mol/L in DI water. **B.** Peak values of the positive and negative voltage peaks for different analytes and the ratio between the positive and negative peak values.